S3–01

Numerical Evaluation of Fatigue Crack Growth Rate of Hot–Rolled 16Mn Steel Based on Compliance Method

Song Hak Jin[*], *Jon Sun Jong*

School of Mechanical Science and Technology, Kim Chaek University of Technology, Pyongyang, DPRK
[*]Corresponding author: Email: shj7641@star–co. net. kp

Summary

Reliable evaluation of the fatigue crack growth rates in different kinds of specimen is necessary for design of engineering components working in fatigue load conditions. A new numerical model for evaluation of the fatigue crack growth rate in a three–point–bend specimen was proposed on the basis of compliance method. A three–point–bending fatigue test machine with strain–controlled loading system was developed to measure decrease of the fatigue load due to increase of the compliance of the specimen caused by crack growth. Evaluation of fatigue crack growth rate of hot–rolled 16Mn steel was conducted by using the test machine and the numerical model. The analysis results of the crack growth rates revealed different tendencies of slope at the former and latter processes of the subcritical propagation. Paris's constants of hot–rolled 16Mn steel for the former process were obtained as $c=1.17\times10^{-9}$ and $m=4.47$, whereas the same parameters for the latter process were obtained as $c'=3.09\times10^{-5}$ and $m'=0.84$. Threshold value of the stress intensity factor range for the material was determined as $\Delta K_{th}=10.8\text{MPa}\cdot\text{m}^{1/2}$.

Keywords: Crack Growth Rate; 16Mn Steel; Compliance Method; Stress Concentration;

1. Introduction

The modeling of damage and fracture is one of the dominant research areas in solid mechanics today. Generally, failures of engineering components could be identified with three stages: crack initiation, subcritical crack growth and final fracture. Considerable theoretical and experimental studies on the first and second stages were carried out for reliable prediction of fatigue lifetime of the engineering components.

Most of the studies on the initiation and propagation of the crack were performed on the basis of quantitative analysis of damage accumulation at the area of stress concentration in the structures. Different approaches were proposed for modeling of the damage accumulation in those processes. Liu et al. suggested a simple model for the crack growth on the basis of Lemaitre's theory of fatigue damage and fracture mechanics [1]. Similar numerical analysis of the crack growth using cohesive zone model under cyclic loading is proposed to develop a coupled predictive approach of crack growth in single crystal [2]. The process of material damage during fatigue crack growth was described using an irreversible cohesive zone model, which governs the separation of the crack flanks and eventually leads to the formation of free surfaces. Seifert and Riedel described the damage accumulation in the vicinity of crack tip by combination of a viscoplastic model with kinematic hardening and a porous plasticity model [3]. This model could explain creep, relaxation and the Bauschinger effect as well as the tension–compression asymmetry often observed for cast iron. Fournier et al. proposed a model for the prediction of the high temperature creep–fatigue lifetime of steels [4~6]. This model was built on the basis of the physical mechanisms responsible for damage due to the interaction of creep, fatigue and oxidation. Meanwhile, the damage accumulation in the pre–fracture zone of three–point–bend specimen under low–cyclic loading was investigated via experimental way, where residual deflection of the specimen was used as the measure of material damage [7]. The other experimental approach to investigate the damage accumulation around notch was conducted using a noncontact digital image measurement system [8]. This system incorporated a contrast correlation method to evaluate the level of plastic damage at each point of the studied area of the specimen from two images acquired before and after the introduction of fatigue deformation.

Evaluation of the crack growth rate at the subcritical propagation process still remains one of the main questions in the fatigue theory. Many studies described the crack propagation behavior using Paris–Erdogan law, where the range of stress intensity factor could be replaced by different parameters such as *J*–integral or strain energy release rate for specific cases [9, 10, 13, 17]. The crack growth rate could be affected by not only the range of stress intensity factor but also the stress ratio, frequency and holding time of the fatigue load [4, 20, 21]. Effect of shape of the specimen, shape and size of the plastic region on the crack growth rate was also studied for different load conditions [14, 22].

Assessment of fatigue crack growth rate was accompanied with experimental measurement of the crack length. A general way to measure the crack length is to observe the crack propagation process using an optical or electronic microscope. Replica method was adopted for measuring the length of macrocracks using optical microscope [11~15], whereas initiation and propagation of microcracks was observed using SEM [15–18]. The crack size around notch tip of different kinds of specimens could be also determined by electrical potential method using Johnson's equation on the basis of ASTM E647 [23~27]. The other way to determine the crack length in the fatigue test process was to use the compliance method based on direct or indirect relation between the crack length and several parameters such as fatigue load, COD or deflection, which were measured during the whole process [21, 28~30]. High accuracy of the modern devices for measurement of the relevant parameters encourages improvement of the reliability of the evaluation of fatigue crack growth rate based on the compliance method.

In the present study, a new numerical model for the evaluation of fatigue crack growth rate in a three–point–bend specimen is proposed on the basis of compliance method. A bending fatigue test machine with strain–controlled loading system was developed for the study.

2. Material and experimental method

The material used in the present study was hot–rolled 16Mn steel. The chemical composition in weight percentage and mechanical properties of hot–rolled 16Mn steel are given in Tab. 1 and 2.

Table 1. Chemical composition of the test material (wt%)

C	Mn	Cr	P	S	Si	Ni	Mo
0.13	1.48	0.004	0.02	0.03	0.46	0.18	0.016

Table 2. Mechanical properties of the test material

σ_s, MPa	σ_b, MPa	δ, %	K_{IC}, MPa/m$^{1/2}$
345	537	21	62.6

Three–point–bend specimens with a height of 20mm, a width of 10mm and a length of 100mm were used to measure the fatigue crack growth rate. Every tested specimen had a notch with a length of 5mm in the middle of the span.

A bending fatigue test machine with strain–controlled loading system was developed for the evaluation of the fatigue crack growth rate in the three–point–bend specimen.

The machine was designed to control the mean value and amplitude of the bending displacement at the centre of the specimen by adjusting preliminary deflection at the free end of the lever and eccentric stroke of the cam. This kind of flexible cam–lever system was adopted to increase adjusting range of displacement at the specimen. The fatigue load generated by the displacement was recorded at an acquisition rate of 300Hz via the 20kN load cell fabricated by HBM.

Using the sinusoidal waveform of the fatigue load with the frequency of 5Hz, the tests were carried out at three load schemes with different minimum deflections (preliminary deflections at the free end of the lever) of 1mm, 1.5mm and 2mm for the same amplitude (the half of eccentric stroke of the cam) of 2.5mm.

3. Compliance model

When a three–point–bend specimen is tested at the bending fatigue test machine with strain–controlled loading system the fatigue load decreases with the progress of the test because of the loss of stiffness of the specimen.

The loss of stiffness of the specimen can be caused by two essential reasons; first, decrease in apparent Young's modulus of the material due to damage accumulation at the region of stress concentration; second, increase in compliance (reciprocal of geometric stiffness) of the specimen due to crack growth [28, 29].

Stress concentration generated at the area around the notch (or crack) tip of the specimen subjected to low cycle fatigue load causes accumulation of damage of the region, which leads to gradual decrease in apparent Young's modulus of the material of the specimen. Modeling of this phenomenon can be conducted by using the recorded measurement results of the fatigue load which exhibit decreasing tendency with the number of cycle.

When the damage accumulated at the region of stress concentration exceeds a specific limit after a certain number of cycles of the fatigue load, a microcrack is generated at the tip of the notch and grows into a macrocrack with the further cycles. This process of the crack growth causes the increase in compliance of the specimen, which is observed as rapid decrease in fatigue load acting on the specimen.

Considering that the specimen is subjected to the maximum fatigue load at the moment of maximum eccentric stroke of the cam, the maximum deflection at the free end of the lever can be determined as

$$\Delta_0 + \Delta_a = \frac{1}{\alpha} C_L F_{\max} + \alpha\left[(C_S + C_F)F_{\max} + \Delta_p\right] \tag{1}$$

where Δ_0 is minimum deflection of the lever, Δ_a is eccentric stroke of the cam, Δ_p is plastic deflection at the centre of the specimen, α is amplification factor of the lever, $F_{\max}$ is the maximum fatigue load acting on the specimen, C_L, C_S and C_F are the compliances of the lever, specimen and load cell, respectively. Based on Eq. (1), the compliance of the specimen C_S can be obtained from the fatigue load measured at the test process. The increment of plastic deflection of the specimen at every load cycle is assumed to be zero and to be proportional to the size of plastic region around the crack tip before and after generation of the crack, respectively. The height of the plastic region across the crack section of the specimen at the maximum fatigue load of every cycle can be obtained as [29].

$$r_0 = \frac{(1-2\nu)^2}{2\pi}\left(\frac{K_{\mathrm{I}max}}{\sigma_s}\right)^2 \tag{2}$$

where ν and σ_s are Poisson' ratio and yield stress of the material of the specimen $K_{I\max}$ is maximum stress intensity factor at the crack tip of the specimen at every cycle.

The maximum stress intensity factor at the crack tip of the three–point–bend specimen can be determined as [29].

$$K_{I\max} = \frac{F_{\max} S}{BW^{3/2}}\left[2.9\left(\frac{a}{W}\right)^{1/2} - 4.6\left(\frac{a}{W}\right)^{3/2} + 21.8\left(\frac{a}{W}\right)^{5/2} - 37.6\left(\frac{a}{W}\right)^{7/2} + 38.7\left(\frac{a}{W}\right)^{9/2}\right] \tag{3}$$

where S, B and W are the span, width and height of the specimen, respectively.

Evaluation of the fatigue crack growth rate was done on the basis of strain energy theory of the linear elastic fracture mechanics. For the strain–controlled fatigue test, relation between the maximum stress intensity factor at the crack tip of the specimen under the plane strain state and the compliance can be expressed as [29].

$$K_{I\max}^2 = \frac{EF_{\max}^2}{2B(1-\nu^2)}\frac{\partial C_S}{\partial a} \tag{4}$$

where a is the crack length, E is Young's modulus of the material of the specimen.

Substituting Eq. (3) into (4), we can obtain the derivative of the compliance of the specimen with respect to the crack length as follows.

$$\frac{\partial C_S}{\partial a}=\frac{2(1-\nu^2)S^2}{EBW^3}\left[8.4\left(\frac{a}{W}\right)-26.7\left(\frac{a}{W}\right)^2+147.6\left(\frac{a}{W}\right)^3-\right.$$
$$-418.7\left(\frac{a}{W}\right)^4+1\,045.6\left(\frac{a}{W}\right)^5-1\,995.4\left(\frac{a}{W}\right)^6+ \quad (5)$$
$$\left.+3101.1\left(\frac{a}{W}\right)^7-2\,910.2\left(\frac{a}{W}\right)^8+1\,497.7\left(\frac{a}{W}\right)^9\right]$$

The Eq. (5) says that the crack growth causes the increase in compliance of the specimen, which implies the possibility to evaluate the crack growth rate at the fatigue test process for the three–point–bend specimen.

4. Test results and discussion

Maximum and minimum forces at every cycle were obtained for three load schemes to evaluate compliance of the specimens and stress intensity factor range in the crack propagation process.(Fig. 1)

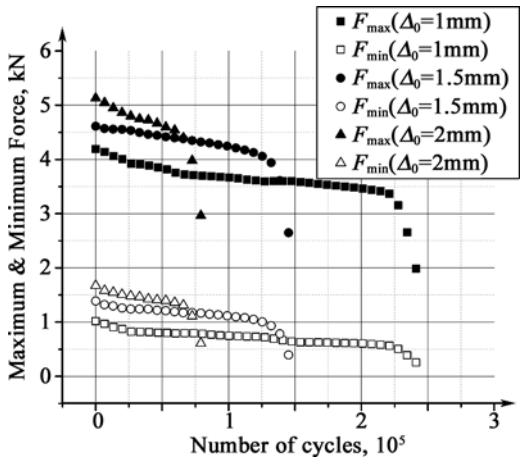

Figure 1. Maximum and minimum forces at every load scheme

Fig. 1 exhibits decreasing tendency of both the maximum and minimum forces with the number of cycles of fatigue load for every scheme.

At the first stages of the tests (before the initiation of the crack), the curves show slow decreasing rate of the fatigue loads, which can be explained as decrease in apparent Young's modulus of the material of the specimen due to damage accumulation at the region of stress concentration around the notch tip. Fitting the curves of Fig. 1, the apparent Young's moduli of the specimens at every load scheme can be expressed as the functions of number of cycles, i.e.

$$\begin{aligned} E(N)&=E_0(1-4.92\times10^{-7}N) \quad (\Delta_0=1\,\text{mm})\\ E(N)&=E_0(1-8.36\times10^{-7}N) \quad (\Delta_0=1.5\,\text{mm})\\ E(N)&=E_0(1-1.86\times10^{-6}N) \quad (\Delta_0=2\,\text{mm}) \end{aligned} \quad (6)$$

where E_0=1.96×10^{5}MPa is Young's modulus of undamaged material(hot rolled 16Mn steel).

At the second stages of the tests (during the crack propagation process), the curves show rapid decreasing rate of the fatigue load, this can be explained as the increase in compliance of the specimen due to the crack growth.

Substituting the measured maximum forces (solid curves at the Fig. 1) into the Eq. (1), we can obtain the curves which show the variation of compliances of the specimens in the test processes.(Fig. 2) During the solution process of the Eq. (1), Δ_0 the preliminary deflection of the lever was taken as 1 mm, 1.5 mm and 2mm for three load schemes, respectively; Δ_a the eccentric stroke of the cam was taken as 5 mm; α the amplification factor of the lever was taken as 7; C_L and C_F the compliances of the lever and load cell were taken as 4.42×10^{-7}m/N and 6.67×10^{-9}m/N, respectively. The coefficients of proportion for calculation of the plastic deflections Δ_p from the size of plastic region were selected by taking account of final plastic deflections of the specimens measured at the end of the tests, which were 0.94, 0.87 and 0.70mm, respectively. The size of plastic region around the crack tip was calculated from the Eq. (2), where σ_s and ν, the yield stress and Poisson' ratio of hot rolled 16Mn steel were taken as 345MPa and 0.3, respectively.

The increment of crack length at every cycle can be determined by integrating the differential Eq. (5) for the curves of compliances depicted in Fig. 2.

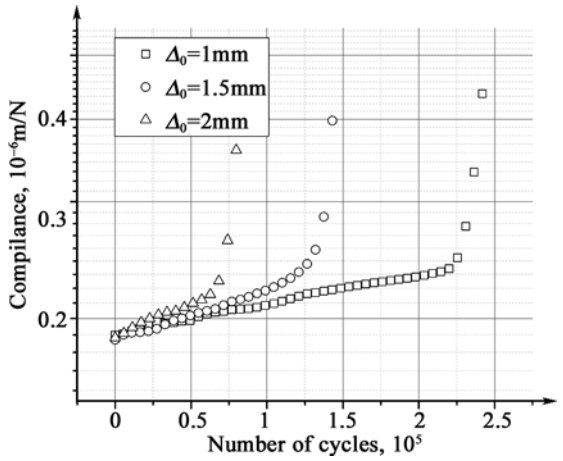

Figure 2. Variation of compliances of the specimens at every load scheme

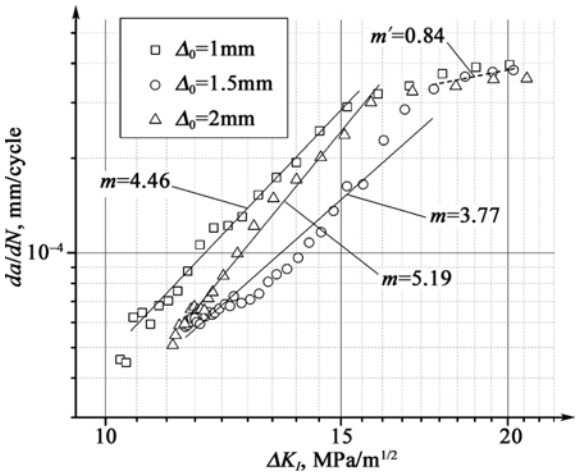

Figure 3. Relation between crack growth rate and stress intensity factor range

In the integral procedure, Young's moduli of the materials of the specimens should be taken as functions of time as denoted in the Eq. (6).

On the basis of calculation results of the crack length, the relations between crack growth rates and stress intensity factor ranges were obtained for three load schemes as shown in Fig. 3. According to Paris's law, these relations can be modeled as [9]

$$\frac{da}{dN} = c\left(\Delta K_I\right)^m \tag{7}$$

where c and m represent the material constants. The curves of Fig. 3 show that the crack propagation processes in the three–point–bend specimens subjected to strain–controlled fatigue load consist of two stages; first stage of rapid propagation and second stage of relatively slow propagation. The material constants c and m for the first stage were obtained by linear fitting of the early parts of the curves, i.e. c=1.58×10^{-9}, m=4.46 for Δ_0=1mm; c=5.50×10^{-9}, m=3.77 for Δ_0=1.5mm; c=1.91×10^{-10}, m=5.19 for Δ_0=2 mm, respectively. The representative material constants for the first stage were chosen as the average values of above constants, i.e. c=1.17×10^{-9}, m=4.47. In contrast with these results, material constants for the second stage represented relatively slow slope, i.e. c'=3.09×10^{-5}, m'=0.84, which were almost similar for three different load schemes. Threshold value of the stress intensity factor range for the material was obtained as ΔK_{th}=10.8 MPa√m from the calculation results. (Fig. 3)

The reason why the crack growth rate decreases at the second stage can be explained in two ways;

First, the partial plane strain state at the area around the crack tip changes to complete plane stress state at a certain crack length; second, strain–controlled loading condition causes decrease in fatigue load along with the crack propagation, which results in relatively slow crack growth rate.

5. Conclusions

Numerical evaluation of crack growth rate of hot–rolled 16Mn steel has been conducted by using a bending fatigue test machine with strain–controlled loading system. A new numerical model to evaluate the fatigue crack growth rate was proposed on the basis of compliance method.

The analysis results of the crack growth rate revealed different tendencies of slope at the former and latter processes of the subcritical propagation. Paris's constants of hot–rolled 16Mn steel for the former process were obtained as c=1.17×10^{-9} and m=4.47, whereas the same parameters for the latter process were obtained as c'=3.09×10^{-5} and m'=0.84. Threshold value of the stress intensity factor range for the material was determined as ΔK_{th}=10.8MPa·m$^{1/2}$.

Acknowledgements

The authors are grateful to NCST (National Committee of Science and Technology) for giving a financial support what is necessary for the development of the bending fatigue test machine with strain–controlled loading system.

References

1. Liu Guoshou, Wang Shiyue, Yang Xijie, 2012, A simple numerical simulation of crack growth rate, *Procedia Engineering.*, 31, 557–562.

2. Bouvard J. L., Chaboche J. L., Feyel F., Gallerneau F., 2009, A cohesive zone model for fatigue and creep–fatigue crack growth in single crystal superalloys, *International Journal of Fatigue* 31, 868–879.

3. Seifert T., Riedel H., 2010, Mechanism–based thermomechanical fatigue life prediction of cast iron. Part I: Models, *International Journal of Fatigue* 32, 1 358–1 367.

4. Fournier B., Sauzay M., Caes C., Noblecourt M., Mottot M., Bougault A., Rabeau V., 2008, Creep–fatigue–oxidation interactions in a 9Cr–1Mo martensitic steel. Part I: Effect of tensile holding period on fatigue lifetime, *International Journal of Fatigue* 30, 649–662.

5. Fournier B., Sauzay M., Caes C., Noblecourt M., Mottot M., Bougault A., Rabeau V., 2008, Creep–fatigue–oxidation interactions in a 9Cr–1Mo martensitic steel. Part III: Lifetime prediction, *International Journal of Fatigue* 30, 1 797–1 812.

6. Fournier B., Salvi M., Dalle F., De Carlan Y., Caes C., Sauzay M., Pineau A., 2010, Lifetime prediction of 9–12%Cr martensitic steels subjected to creep–fatigue at high temperature, *International Journal of Fatigue* 32, 971–978.

7. Kornev Vladimir, Karpov Evgeniy, Demeshkin Alexander, 2010, Damage accumulation in the pre–fracture zone under low–cyclic loading of specimens with the edge crack, *Procedia Engineering* 2, 465–474.

8. Diaz F. V., Armas A. F., Kaufmann G. H., Galizzi G. E., 2004, Nondestructive evaluation of the fatigue damage accumulation process around a notch using a digital image measurement system, *Optics and Lasers in Engineering* 41, 477–487.

9. Paris P. C, Erdogan F., 1960, A critical analysis of crack propagation laws, *J. Basic Eng*, 85, 528–534.

10. HU Hong–jiu, GUO Xing–ming, LI Pei–ning, XIE Yu–jun, LI Jie, 2006, A New Cyclic *J*–Integral for Low–Cycle Fatigue Crack Growth, *Applied Mathematics and Mechanics* (English Edition), 27(2), 149–160.

11. Shuhei Nogami, Yuki Sato, Akira Hasegawa, 2010, Fatigue Life Assessment Based on Crack Growth Behavior in Reduced Activation Ferritic/Martensitic Steel, *Journal of NUCLEAR SCIENCE and TECHNOLOGY* 47(5), 457–461.

12. Yukitaka Murakami, Md. Shafiul Ferdous, Chobin Makabe, 2016, Low cycle fatigue damage and critical crack length affecting loss of fracture ductility, *International Journal of Fatigue* 82, 89–97.

13. Hutar P., Kubena I., Sevcik M., Smid M., Kruml T., Nahlik L., 2014, Small fatigue crack propagation in Y_2O_3 strengthened steels, *Journal of Nuclear Materials* 452, 370–377.

14. Shuhei Nogami, Yuki Sato, Akira Hasegawa, Hiroyasu Tanigawa, 2011, Effect of specimen shape on micro–crack growth behavior under fatigue in reduced activation ferritic/martensitic steel, *Journal of Nuclear Materials* 417, 131–134.

15. Chen Q., Kawagoishi N., Nisitani H., 2000, Evaluation of fatigue crack growth rate and life prediction of Inconel 718 at room and elevated temperatures, *Materials Science and Engineering A*277, 250–257.

16. Zhu S.J., Peng L.M., Moriya T., Mutoh Y., 2000, Effect of stress ratio on fatigue crack growth in TiAl intermetallics at room and elevated temperatures, *Materials Science and Engineering A*290, 198–206.

17. Wang Hongtao, Sun Libin, Li Chenfeng, Shi Li, Wang Haitao,

2012, An evaluation on fatigue crack growth in a fine–grained isotropic graphite, *Nuclear Engineering and Design* 250, 197–206.

18. Knobbe Helge, Köster Philipp, Christ Hans–Jürgen, Fritzen Claus–Peter, Riedler Martin, 2010, Initiation and Propagation of Short Fatigue Cracks in Forged Ti6Al4V, *Procedia Engineering* 2, 931–940.

19. Chan Kwai S., Jones Peggy, Wang Qigui, 2003, Fatigue crack growth and fracture paths in sand cast B319 and A356 aluminum alloys, *Materials Science and Engineering A*341, 18–34.

20. Oda Yasuji, Noguchi Hiroshi, Higashida Kenji, 2011, Loading Frequency Effect on Fatigue Crack Growth Rate in Low Pressure Hydrogen Gas in the Case of A6061–T6 Aluminum Alloy, *Journal of Solid Mechanics and Materials Engineering* 5(11), 599–609.

21. Shaifulazuar Rozali, Yoshiharu Mutoh, Kohsoku Nagata, 2009, Effect of Stress Ratio on Fatigue Crack Growth Behavior of Magnesium Alloy AZ61 under 3.5 Mass% NaCl Spray Environment, *Journal of Solid Mechanics and Materials Engineering* 3(12), 1 274–1 284.

22. Vansovich K. A., Yadrov V. I., Beseliya D.C., 2015, The effect of stress state characteristics on the surface fatigue cracks growth rate taking into account plastic deformations, *Procedia Engineering* 113, 244–253.

23. Dogan B., Ceyhan U., Petrovski B., 2007, High temperature crack initiation and defect assessment of P22 steel weldments using time dependent failure assessment method, *Engineering Fracture Mechanics* 74, 839–852.

24. Sugiura R., Yokobori A.T. Jr., Tabuchi M., Yokobori T., 2007, Comparison of creep crack growth rate in heat affected zone of welded joint for 9%Cr ferritic heat resistant steel based on C*, d*d*/dt, *K* and *Q** parameters, *Engineering Fracture Mechanics* 74, 868–881.

25. Akio Fuji, A. Toshimitsu Yokobori Jr, Mizuki Kikuchi, Masaaki Tabuchi, 2003, Effect of microstructure on the characterization of creep crack growth rate and rupture in TiAl intermetallic alloys, *International Journal of Pressure Vessels and Piping* 80, 435–440.

26. Silva J. M., Claudio R. A., Branco C. Moura, Ferreira J., 2010, Creep–fatigue behavior of a new generation Ni–base superalloy for aeroengine usage, *Procedia Engineering* 2, 1 865–1 875.

27. Liu Xingbo, Kang Bruce, Chang Keh–Minn, 2003, The effect of hold–time on fatigue crack growth behaviors of WASPALOY alloy at elevated temperature, *Materials Science and Engineering A*340, 8–14.

28. 2000, Mechanical Testing and Evaluation, *ASM HANDBOOK* Vol. 8, 1 705–1 747.